A Three-Dimensional Linear Response Model of the Tropical Intraseasonal Oscillation

By Y. Hayashi

Geophysical Fluid Dynamics Laboratory/NOAA, Princeton University, Princeton NJ 08542, USA

and

Saburo Miyahara

Department of Physics, Kyushu University, Fukuoka 812, Japan
(Manuscript received 1 June 1987, in revised form 24 October 1987)

Abstract

The propagation and structure of the tropical intraseasonal oscillation are studied by the use of a three-dimensional linear response model and compared with those obtained from the FGGE data.

It is assumed that the imposed thermal forcing oscillates with a 40 day period and propagates eastward. Although the amplitude of the forcing is assumed to be large over a certain longitude band and small elsewhere, the responding zonal wind oscillation has significant components that propagate eastward around the earth as observed. This oscillation is also associated with an observed longitudinal node in the region of the maximum forcing. When the imposed forcing is strictly confined over some longitudes, the zonal wind oscillation propagates eastward and westward away from the forced region as in the case of a two-dimensional model. The eastward moving wavenumber 1 component is associated with the observed wave pattern of the combined Kelvin-Rossby mode in the upper troposphere, while it is dominated by that of the Rossby mode in the lower troposphere. This component also takes the observed structure of the Walker cell modified by a frictional meridional convergence in the boundary layer. The dominance of the Rossby mode in the lower troposphere is due to the effect of surface friction.

1. Introduction

The tropical intraseasonal oscillation found by Madden and Julian (1971) is one of the current subjects of intensive study. Madden and Julian (1972) suggested that this oscillation takes the form of a planetary-scale Walker (zonal-vertical) cell and propagates eastward, presumably with an eastward propagating convective heating. Yasunari (1980, 1981) found that this oscillation propagates northward in the summer monsoon region and suggested that it is associated with local meridional-vertical (Hadley) circulations. Maruyama (1982) showed that this eastward propagating oscillation is also associated with longitudinal nodes and antinodes. Anderson and Rosen (1983) detected a 40–50 day oscillation in the zonal velocity. Goswami and Shukla (1984) detected a 20–40 day oscillation in a zonally symmetric general circulation mdoel, while Hayashi and Sumi (1986) found a 30–40 day oscillation in an all ocean surface general circulation model. Lorenc (1984) and Krishnamurti *et al.* (1985) detected an eastward propagation of the intraseasonal divergence field, while Weickmann (1983), Knutson *et al.* (1986) and Nakazawa (1986) showed an eastward propagation of the intraseasonal outgoing longwave radiation which is interpreted as a measure of convective activity. Murakami *et al.* (1984) studied the three-dimensional phase propagation and structure of the 40–50 day oscillation and concluded that its major energy source was the

conversion of potential energy into kinetic energy.

Parker (1973) interpreted this oscillation as the theoretical Kelvin mode studied by Matsuno (1966), although the vertical scale of the low frequency Kelvin wave in the absence of heating is unrealistically small. Chang (1977) suggested that the observed vertical scale can be explained by the effect of strong viscosity even in the absence of heating. Yamagata and Hayashi (1984), by modifying a two-dimensional linear response model of Gill (1980), demonstrated that the eastward moving Kelvin mode and the westward moving Rossby mode are excited to the east and west, respectively, of a localized thermal forcing which pulsated with a prescribed 40-day period. However, there is the possibility that the heating itself propagates as a result of mutual interaction between large-scale waves and cumulus convection as in the wave–CISK model (Hayashi, 1970; Lindzen, 1974; Lau and Peng, 1987; Miyahara, 1987; Yamagata, 1987; Takahashi, 1987). There is also the possibility that the intraseasonal oscillations result from interactions with ocean or ground hydrology as suggested by dynamical mdoels (Webster and Chou, 1980; Webster, 1983).

Recently, Hayashi and Golder (1986, 1987) have made space-time spectral and filter analyses of the tropical intraseasonal oscillation appearing in the FGGE IIIb data and a GFDL 30-wavenumber spectral general circulation model without air-sea interactions. The observed and simulated intraseasonal oscillations were characterized by a spectral peak at wavenumber 1 and periods of 40–50 days with an eastward phase velocity. The global eastward phase propagation was detected both in the wind and precipitation which were associated with longitudinal nodes and antinodes. This oscillation takes the form of the combined Kelvin-Rossby mode in the upper troposphere, while it is dominated by the Rossby mode in the lower troposphere. It also takes the form of the zonal-vertical (Walker) cell with a latitudinal tilt, except that the boundary layer convergence is modified by a meridional convergence. It was also demonstrated that the tropical intraseasonal oscillations disappeared from a model without condensational heating, while extratropical intraseasonal oscillations still appeared in the absence of the tropical intraseasonal oscillations.

The present paper is intended to examine whether the propagation and structure of the observed tropical intraseasonal oscillation can be better simulated by a three-dimensional linear response model in which a nearly localized eastward propagating heat source is prescribed. This improves on the two-dimensional linear response model of Yamagata and Hayashi (1984) which assumed a strictly localized heat pulsation. The three-dimensional model is described in Section 2, while Section 3 compares the numerical results with those obtained from the FGGE IIIb data processed at GFDL. Conclusions and remarks are given in Section 4.

2. Model

The model is based on the linearized equations in the absence of a basic flow on an equatorial beta plane with log-pressure coordinates as given by

$$\frac{\partial u}{\partial t}-\beta y v=-\frac{\partial \phi}{\partial x}-\varepsilon u+\frac{\partial}{\partial z}\left(K_e\frac{\partial u}{\partial z}\right), \quad (1)$$

$$\frac{\partial v}{\partial t}+\beta y u=-\frac{\partial \phi}{\partial y}-\varepsilon v+\frac{\partial}{\partial z}\left(K_e\frac{\partial v}{\partial z}\right), \quad (2)$$

$$\frac{\partial}{\partial t}\left(\frac{\partial \phi}{\partial z}\right)+N^2 w=\frac{\kappa}{H}J-\gamma\frac{\partial \phi}{\partial z}, \quad (3)$$

$$\frac{\partial u}{\partial x}+\frac{\partial v}{\partial y}+\frac{1}{p}\frac{\partial pw}{\partial z}=0, \quad (4)$$

where the notations are conventional (see Holton, 1975) except for the Rayleigh friction coefficient (ε), the vertical eddy diffusion coefficient (K_e), and the Newtonian cooling coefficient (γ).

Eliminating w, the above equations are Fourier transformed in longitude and time as

$$(i\omega+\varepsilon)u_{k,\omega}-\frac{\partial}{\partial z}\left(K_e\frac{\partial u_{k,\omega}}{\partial z}\right)-\beta y v_{k,\omega}+ik\phi_{k,\omega}=0, \quad (5)$$

$$(i\omega+\varepsilon)v_{k,\omega}-\frac{\partial}{\partial z}\left(K_e\frac{\partial v_{k,\omega}}{\partial z}\right)+\beta y u_{k,\omega}+\frac{\partial \phi_{k,\omega}}{\partial y}=0, \quad (6)$$

$$iku_{k,\omega}+\frac{\partial v_{k,\omega}}{\partial y}-\frac{1}{p}\frac{\partial}{\partial z}\left[\frac{p}{N^2}(i\omega+\gamma)\frac{\partial \phi_{k,\omega}}{\partial z}\right]$$
$$=-\frac{1}{p}\frac{\partial}{\partial z}\left(\frac{p\kappa}{N^2H}J_{k,\omega}\right), \quad (7)$$

where $u_{k,\omega}$, $v_{k,\omega}$, $\phi_{k,\omega}$, and $J_{k,\omega}$ are the Fourier coefficients for the zonal wavenumber k and angular frequency ω defined by

$$(u, v, \phi, J)=Re\sum_{k}\sum_{\omega}(u_{k,\omega}, v_{k,\omega}, \phi_{k,\omega}, J_{k,\omega})\cdot\exp(ikx+i\omega t). \quad (8)$$

The thermal forcing J is assumed to vanish above $z = Z_b$ and below $z = Z_a$, while it takes the following form in the heating layer:

$$J=ReA(x)B(x-ct)\cdot\exp\left[-\left(\frac{y}{L_y}\right)^2\right]\sin\left[\frac{\pi(z-Z_a)}{Z_b-Z_a}\right]. \quad (9)$$

Here, the function A(x) represents a zonal variation of the amplitude defined by

$$A(x)=\cos\left(\frac{\pi x}{L_x}\right)+a \quad \text{for } |x|\leqq L_x, \quad (10a)$$
$$=a \quad \text{for } |x|>L_x. \quad (10b)$$

It should be noted that A(x) varies from 1+a to a.

The function B(x − ct) represents the phase propagation with phase speed c. This function can essentially be represented by a sinusoidal function $\exp(iK_px+i\omega t)$ with zonal wavenumber 1, since the observed intraseasonal heating oscillation is associated with one positive anomaly and one negative anomaly along a latitude circle (see Fig. 6a, b of Knutson and Weickmann, 1987). It is, however, more realistic to represent it by a more localized function which gives a shorter (or larger) longitudinal distance between the positive and negative anomalies than a half latitude circle.

When A(x) is expanded in a zonal Fourier series as

$$A(x)=\sum_{k=-N}^{N}A_k\exp(ikx), \quad (11)$$

Eq. (9) is reduced to

$$J=Re\sum_{k=-N}^{N}A_k\exp[i(k+K_p)x+i\omega t]\cdot\exp\left[-\left(\frac{y}{L_y}\right)^2\right]\sin\left[\frac{\pi(z-Z_a)}{Z_b-Z_a}\right]. \quad (12)$$

The Fourier transformed equations (5), (6), and (7) are approximated by a finite difference in the y and z coordinates with the lateral increment of 285.7 km.

The log-pressure "z" coordinate is transformed to ζ as

$$z=h_0[\exp(\alpha\zeta)-1], \quad (13)$$

where h_0 = 1.0 km, and α = 0.067.

The vertical increment in ζ is 1.0 with 52 layers in vertical (0–29 km). The actual heights of the levels are listed in Table 1.

The finite difference equations are then solved by an inversion method of Lindzen and Kuo (1969) with the boundary conditions given by

$$v=0 \quad \text{at} \quad y=Y_b, \quad (14)$$
$$u=v=d\phi/dt=0 \quad \text{at} \quad z=0, \quad (15)$$

and

$$u=v=\phi=0 \quad \text{at} \quad z=Z_t.$$

where $d\phi/dt$ is the vertical velocity and is different from "w" in the log-pressure coordinate system (see Holton, 1975, p. 57).

The constant parameters are given by:

Y_b = 4,000 km, Z_t = 29 km, Z_a = 0.7 km, Z_b = 13 km, L_x = 4,444 km, L_y = 3,000 km, N = 0.01 s^{-1}, $\varepsilon^{-1}=\gamma^{-1}=$ 20 days, and K_e = 5 m^2s^{-2}.

Table 1 The actual height of the 52-level model

Model level	z (km)
1	0.0
10	0.83
20	2.57
30	5.98
40	12.64
50	25.66
52	29.48

3. Numerical results

It is assumed that the imposed thermal forcing oscillates with a 40-day period and propagates eastward with a wavenumber 1 phase variation. The forcing has a sinusoidal vertical profile and attains its maximum at 6.5 km and vanishes at 13 km. It has a Gaussian latitudinal profile and attains its maximum at the equator, decaying by a factor of 1/e for y = 3000 km away from the equator (i.e., L_y = 3000 km). The forcing has no vertical or latitudinal phase variation, although the observed convective heating as inferred from the outgoing longwave radiation is associated with some latitudinal phase variation. As illustrated by the longitude-time (a) and longitude-latitude (b) distributions in Fig. 1, the amplitude of the heating oscillation is mostly confined over a longitudinal interval of 80 degrees and is reduced to 28.6% (a = 0.4) of its maximum value (a+1 = 1.4) outside of this interval. This means that the variance of the thermal oscillation is reduced to 8.2% of its maximum variance. The zonal speed of the thermal oscillation following the local maximum is slower (5 m/s) than that outside of this region (12 m/s). The slow local speed is consistent with that (4–5 m/s) of the observed outgoing longwave radiation in the Indian monsoon region (e.g., Knutson *et al.*, 1986, Fig. 5b).

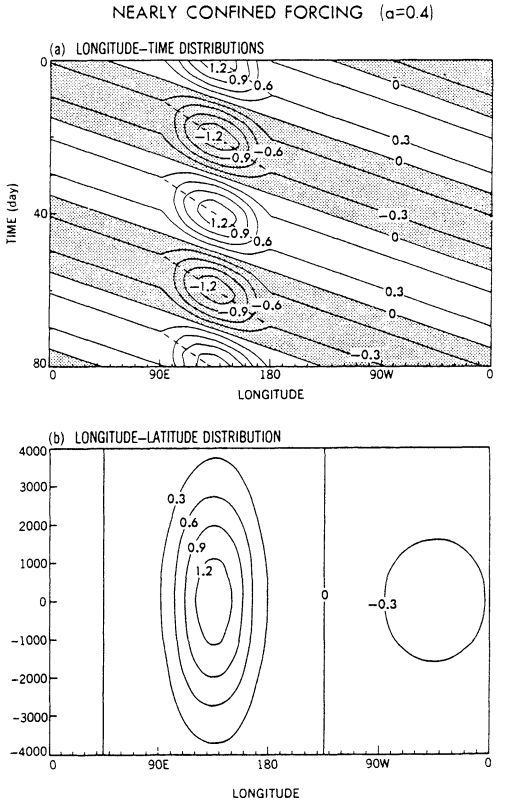

Fig. 1. Longitude-time distribution at the equator (a) and longitude-time distribution at time t=0 (b) of eastward propagating thermal forcing which is nearly confined in longitude (a=0.4).

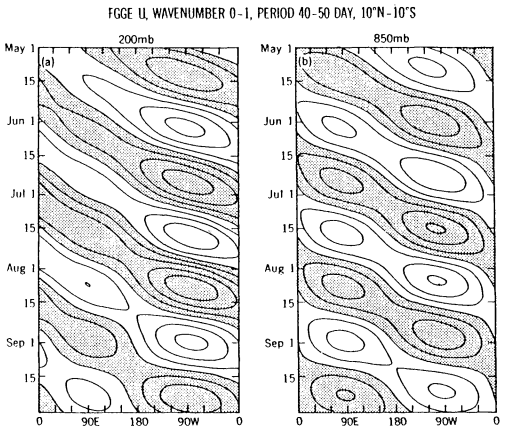

Fig. 2. Longitude-time distributions (GFDL FGGE IIIb, 10°N–10°S average) of the wavenumber 0–1 zonal velocity subjected to a 40–50 day filter at 200 mb (a) and 850 mb (b). Contour intervals are 1 m/s (a), 0.5 m/s (b). Shading indicates positive values.

Figure 2 shows the longitude-time sections at 200 mb (a) and 850 mb (b) of the wavenumber 0-1 zonal velocity (FGGE, 10°S–10°N average) which has been subjected to a 40–50 day time filter. It is seen that this 40–50 day oscillation propagates eastward around the earth with nodes occurring near the 0° and 180° longitudes and antinodes occurring near 90°E and 90°W. The nodes are more clearly seen in a GCM analysis (Hayashi and Golder, 1986, Fig. 4).

In Fig. 3, the longitude-time sections of the model's zonal velocity (0°–10°N average) at 12.5 km (a) and 0.82 km (b) are given. The zonal velocities at these two levels are 180 degrees out of phase, being consistent with the Walker cell. It should be noted that the zonal velocity oscillation propagates eastward around the earth with the observed slow phase velocity (10 m/s) in

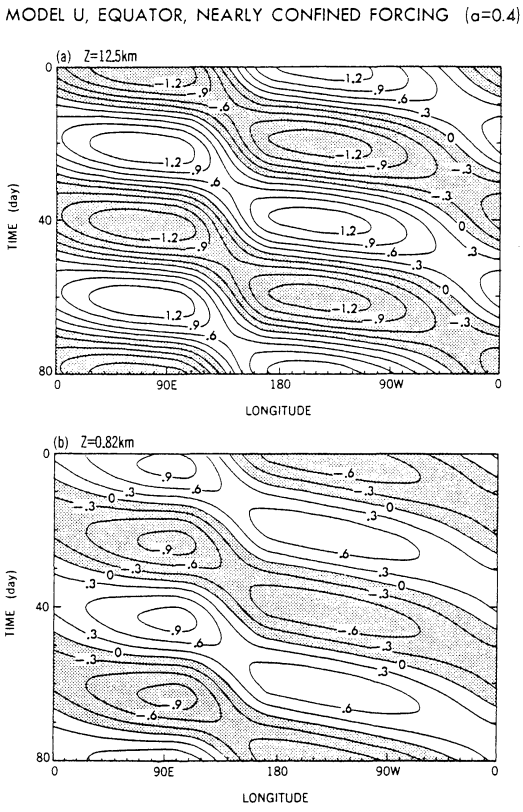

Fig. 3. Longitude-time distributions (model, 10°S–10°N average) of the zonal velocity (m s^{-1}) at 12.5 km (a) and 0.82 km (b) for a=0.4 (heating nearly confined over longitude 100°–180°).

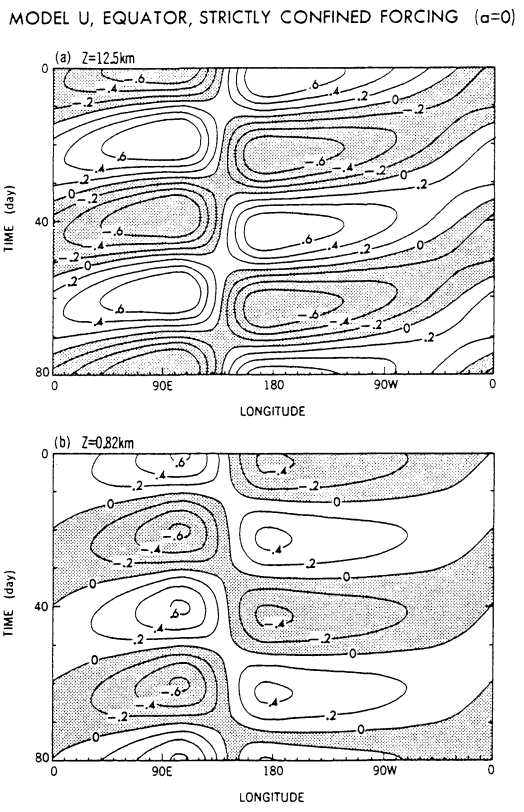

Fig. 4. As in Fig. 3 except for a=0 (heating strictly confined over logitude 100°–180°).

spite of the fact that the thermal forcing is nearly confined. It should also be noted that a node occurs in the region of the confined forcing due to an interference between eastward and westward moving waves forced by the localized heating.

Figure 4 is the same as Fig. 3 except that the propagating heat source is longitudinally restricted (a=0). In this case, the zonal velocity oscillation propagates in a westward direction west of the forcing as had occurred in a two-dimensional model (Yamagata and Hayashi, 1984) which had a localized thermal pulsation. This defect for a=0 is not alleviated by increasing the Rayleigh friction (not illustrated).

Figure 5 illustrates longitude-latitude sections (FGGE, 200 mb and 850 mb) of wavenumber 1 wind vectors and geopotential height contours which are filtered over the 40–50 day period and are composited over May–September along the longitudinal-time isoline of the eastward phase velocity (10.3 m/s) of the 40–50 day oscillation. This space-time composite enhances the eastward moving component over the westward moving component. At 200 mb (Fig. 5a), the wind vectors close to the equator are parallel to the equator, while the zonal velocity is in phase with the geopotential height, being consistent with the Kelvin wave pattern (see Matsuno, 1966, Fig. 8). However, the geopotential height reverses its phase across 15°N. The wave pattern around 30°N resembles the Rossby wave pattern (see Matsuno, 1966, Fig. 4c) in that the wind vectors geostrophically follow the geopotential height contours. At 850 mb (Fig. 5b), the wave pattern is dominated by the Rossby mode.

Figure 6 shows longitude-latitude sections (model) of the eastward moving wavenumber 1 component of the wind vectors and geopotential

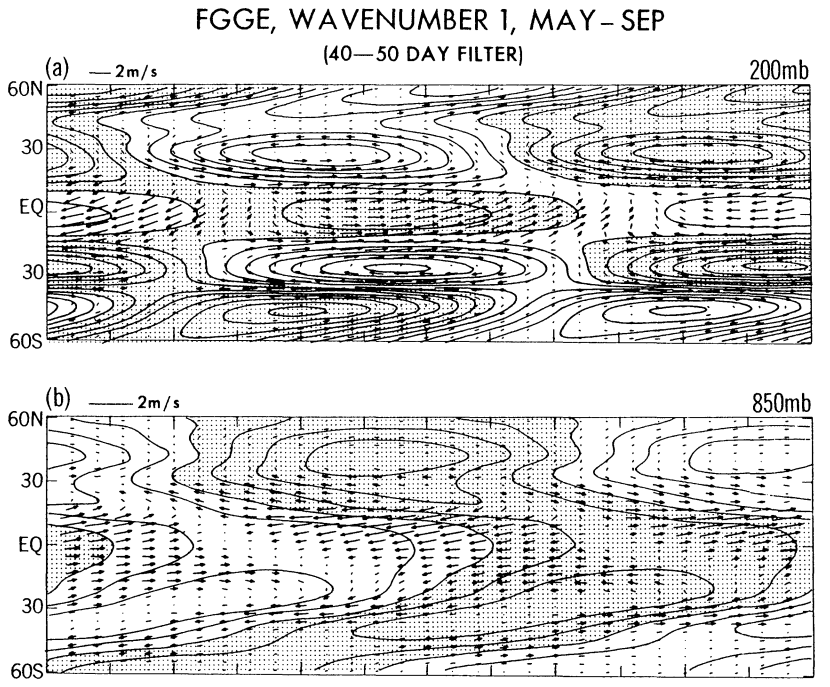

Fig. 5. Longitude-latitude sections (GFDL FGGE) at 200 mb (a) and 850 mb (b) of the wavenumber 1 wind vectors and geopotential height contours which are filtered over the 40–50 day period and are composited over the May–September period along the longitude-time isolines of the phase velocity (10.3 m/s) of the 40–50 day oscillation. Contour interval is 2 m. Shading indicates positive values.

height contours at 13.1 km and 0.82 km. The wave pattern at 13.1 km (Fig. 6a) resembles that of FGGE (Fig. 5a) in that this pattern takes the form of the Kelvin mode near the equator and the Rossby mode away form the equator. However, this pattern is somewhat different from the thermally forced equatorial wave of a two-dimensional model (Matsuno, 1966, Fig. 9; Gill, 1980; Yamagata and Hayashi, 1984) which is not associated with an abrupt latitudinal phase reversal in the geopotential height. The wave pattern at 0.82 km (Fig. 6b) resembles that of FGGE at 850 mb (Fig. 5b) in that this pattern is dominated by the Rossby mode. It also resembles the thermally forced equatorial wave pattern of Matsuno (1966). When the lower boundary condition is modified in such a way that the surface stress vanishes ($\partial u/\partial z=\partial v/\partial z=0$, at $z=0$) , the wave patterns at 0.82 km and 13.1 km (not illustrated) take the form of the Kelvin mode near the equator and the Rossby mode away from the equator.

Figure 7a shows the longitude-latitude sections (FGGE) of the contours of wavenumber 1 vertical velocity at 515 mb and the wind vectors at 200 mb which are filtered over the 40–50 day period and are composited over the May–September period as in Fig. 5. The 515 mb vertical velocity can be interpreted as a measure of the horizontal convergence at 200 mb due to the continuity of mass. It is seen that this horizontal convergence is consistent with that of the Walker cell which is associated with a zonal convergence, as observationally suggested by Madden and Julian (1972). It should be noted, however, that the vertical velocity is associated with a northwest-southeast tilt between 0° and 20°N. Fig. 7b is the same as Fig. 7a except for the vertical velocity at 850 mb and the wind vectors at 1000 mb. The 850 mb vertical velocity can be interpreted as a measure of the horizontal convergence at 1000 mb. It is seen that the horizontla convergence is largely modified by a meridional convergence. In particular, the vertical velocity at 850 mb is not 90 degrees out of phase with the zonal velocity at 1000 mb, being contrary to the Walker cell.

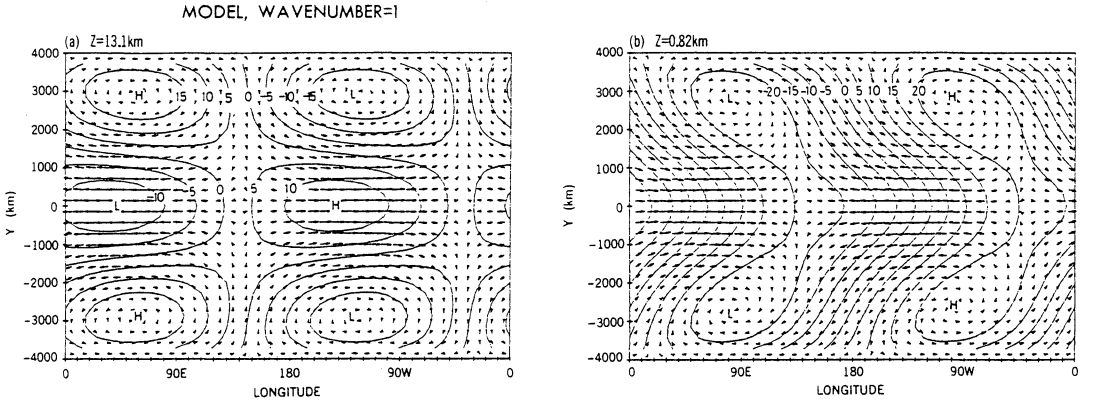

Fig. 6. Longitude-latitude sections (model) on day 0 of the eastward moving wavenumber 1 component of the wind vectors and geopotential height contours (m) at 13.1 km (a) and 0.82 km (b). The scales of the zonal and meridional components of the vectors are proportional to the longitude and latitude scales.

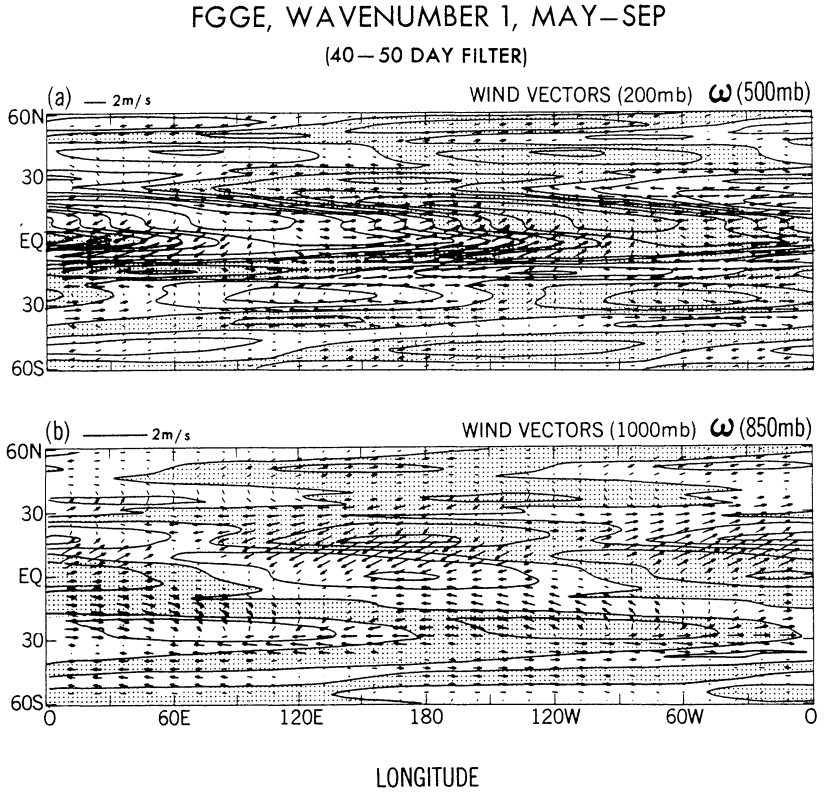

Fig. 7. Longitude-latitude section (GFDL FGGE) of the contours of wavenumber 1 vertical pressure velocity at 515 mb (a) and 850 mb (b), and wind vectors at 200 mb (a) and 1000 mb (b) which are filtered over the 40–50 day period and are composited over May–September as in Fig. 5. Contour interval is 2×10^{-11} Pa/s. Shading indicates downward motion.

Figure 8a shows the longitude-latitude sections (model) of the contours of the eastward moving wavenumber 1 component of the vertical velocity at 5.1 km and wind vectors at 12.5 km. It is seen that the horizontal convergence near the equator is mainly a zonal convergence as in FGGE. Unlike FGGE, however, the vertical velocity at this level is not associated with a meridional tilt, since the imposed heating has no meridional tilt. Fig. 8b is the same as Fig. 8a except for the vertical velocity at 0.82 km and wind vectors at 0.07 km. As in FGGE, the horizontal convergence is largely modified by a meridional convergence. In particular, the low level vertical velocity near the equator is 180 degrees out of phase with the surface zonal velocity, being contrary to the Walker cell.

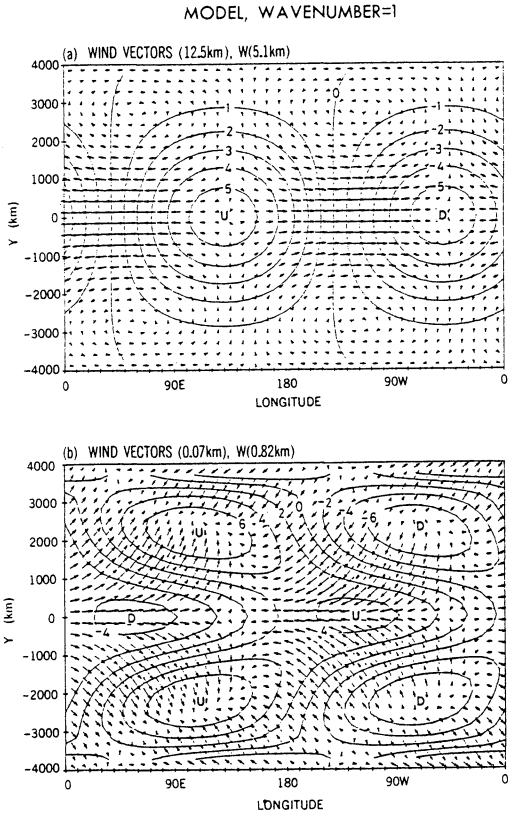

Fig. 8. Longitude-latitude section (model) on day 0 of the contours of wavenumber 1, vertical velocity at 5.1 km (a, 10^{-3} m s^{-1}) and 0.82 km (b, 10^{-4} m s^{-1}), and wind vectors at 12.5 km (a) and 0.07 km (b). The scales of the zonal and meridional components of the vectors are proportional to the longitude and latitude scales.

Interestingly, this low level vertical velocity is associated with a meridional tilt as in FGGE, in spite of the fact that the thermal forcing has no meridional tilt. When the lower boundary condition is modified in such a way that the surface stress vanishes, the meridional convergence in the boundary layer and the meridional tilt disappear (not illustrated). The horizontal pattern of the 5.1 km vertical velocity (Fig. 8a) is similar to and nearly in phase with that of the thermal forcing (see Fig. 1b).

4. Conclusions and remarks

The present paper has studied the propagation and structure of the tropical intraseasonal oscillations by the use of a three-dimensional linear model and has compared them with those obtained from the FGGE data. The main conclusions are summarized as follows:

1) The model's zonal wind oscillation has significant components which propagate eastward around the earth as observed, in spite of the fact that the eastward propagating thermal forcing is nearly confined to given longitudes. This oscillation is also associated with a longitudinal node in the region of the confined thermal forcing. When the forcing is strictly confined over some longitudes, the zonal wind oscillation propagates eastward and westward away from the forced region as in the case of a two-dimensional model.

2) The eastward moving wavenumber 1 component is associated with the observed wave pattern of the combined Kelvin-Rossby mode in the upper troposphere, while it is dominated by that of the Rossby mode in the lower troposphere. The dominance of the Rossby mode in the lower troposphere is due to the effect of surface friction.

3) This component is also associated with the observed structure of the Walker cell modified by a frictional meridional convergence in the boundary layer.

The present study suggests that the thermal forcing must, to some extent, propagate around the earth in order to explain the global propagation of the observed zonal velocity. Even without space and time filtering, the global propagation of the observed outgoing longwave radiation at times can be detected (e.g., Nakazawa, 1986).

The global eastward propagation will also occur in a two-dimensional model with a nearly localized eastward propagating thermal forcing. It should be mentioned that the thermal forcing need not be localized at all for the appearance of the eastward propagating Rossby mode. This mode can appear in both two- and three-dimensional linear models even when the thermal forcing is associated with an eastward moving wavenumber 1.

Although the observed structure has been reasonably well simulated by the present three-dimentional model with a prescribed eastward propagating heat source, the vertical velocity has no meridional tilt except at the lower level where the frictional convergence gives rise to a meridional tilt. This defect can be attributed to the imposed thermal forcing which has no meridional tilt in the presence of surface friction. When the thermal forcing is proportional to the low level vertical velocity as in the wave-CISK therory, the thermal forcing must also have a meridional tilt in the presence of surface friction. In the present linear response model, the wavenumber 0 (i.e. zonal mean) oscillation in the zonal velocity vanishes at the equator, although the thermal forcing and pressure have a zonal mean component. This defect will be alleviated by the use of a nonlinear model. It should also be noted that this linear model did not require a strong internal viscosity to reproduce the observed phase propagation and structure of the tropical intraseasonal oscillation, although a strong viscosity may be required in the linear model to reproduce its amplitude as in the case of tropical stationary waves.

Acknowledgments

The authors are grateful to I. M. Held, R. T. Pierrehumbert and D. G. Golder for their appropriate comments on the original manuscript.

References

Anderson, J.R. and R.D. Rosen, 1983: The latitude-height structure of 40–50 day variations in atmospheric angular momentum. *J. Atmos. Sci.*, **40**, 1584–1591.

Chang, C.P., 1977: Viscous internal gravity waves and low frequency oscillations in the tropics. *J. Atmos. Sci.*, **34**, 901–910.

Gill, A.E., 1980: Some simple solutions for heat-induced tropical circulations. *Quart. J. Roy. Meteor. Soc.*, **106**, 447–462.

Goswami, B.N. and J. Shukla, 1984: Quasi-periodic oscillations in a symmetric general circulation model. *J. Atmos. Sci.*, **41**, 20–37.

Hayashi, Y., 1970: A theory of large-scale equatorial waves generated by condensational heat and accelerating the zonal wind. *J. Meteor. Soc. Japan*, **48**, 140–160.

_____ and D.G. Golder, 1986: Tropical intraseasonal oscillations appearing in a GFDL general circulation model and FGGE data, Part I: Phase propagation. *J. Atmos. Sci.*, **43**, 3058–3067.

_____ and _____, 1987: Tropical intraseasonal oscillations appearing in a GFDL general circulation model and FGGE data, Part II: Structure and moisture effect: Submitted for publication.

Hayashi, Y.Y. and A. Sumi, 1986: The 30–40 day oscillations simulated in an "aqua planet" model. *J. Meteor. Soc. Japan*, **64**, 451–467.

Holton, J.R., 1975: The dynamic meteorology of the stratosphere and mesosphere. *Meteor. Monogr.*, **37**, Amer. Meteor. Soc., 216 pp.

Knutson, T.R., K.M. Weickmann and J.E. Kutzbach, 1986: Global scale intraseasonal oscillations of outgoing longwave radiation and 250 mb zonal wind during northern hemisphere summer. *Mon. Wea. Rev.*, **114**, 605–623.

_____ and K.M. Weickmann, 1987: 30–60 day atmospheric oscillations: composite life cycles of convection and circulation anomalies. *Mon. Wea. Rev.*, **115**, 1407–1436.

Krishnamurti, T.N., P.K. Jayakumar, J. Sheng, N. Surgi and A. Kumar, 1985: Divergent circulations on the 30 to 50 day time scale. *J. Atmos. Sci.*, **42**, 364–375.

Lau, K.M. and L. Peng, 1987: Origin of low frequency (intraseasonal) oscillations in the tropical atmosphere. Part I: Basic theory. *J. Atmos. Sci.*, **44**, 950–972.

Lindzen, R.S., 1974: Wave-CISK in the tropics. *J. Atmos. Sci.*, **31**, 156–179.

_____ and H.L. Kuo, 1969: A reliable method for the numerical integration of a large class of ordinary and partial differential equations. *Mon. Wea. Rev.*, **96**, 732–734.

Lorenc, A.C., 1984: The evolution of planetary scale 200 mb divergent flow during the FGGE year. *Quart. J. Roy. Meteor. Soc.*, **110**, 427–441.

Madden, R.A. and P.R. Julian, 1971: Detection of a 40–50 day oscillation in the zonal wind in the tropical Pacific. *J. Atmos. Sci.*, **28**, 702–708.

_____ and _____, 1972: Description of global-scale circulation cells in the tropics with a 40–50 day period. *J. Atmos. Sci.*, **29**, 1109–1123.

Maruyama, T., 1982: Upper tropospheric zonal wind oscillation with a 30–50 day period over the equatorial western Pacific observed in cloud movement vectors. *J. Meteor. Soc. Japan*, **60**, 172–182.

Matsuno, T., 1966: Quasi-geostrophic motions in the equatorial area. *J. Meteor. Soc. Japan,* **44**, 25–43.

Miyahara, S., 1987: A simple model of the tropical intraseasonal oscillation. *J. Meteor. Soc. Japan,* **65**, 341–351.

Murakami, T., T. Nakazawa and J. He, 1984: On the 40–50 day oscillations during the 1979 northern hemisphere summer. Part I: Phase propagation. *J. Meteor. Soc. Japan,* **62**, 440–468.

Nakazawa, T., 1986: Mean features of 30–60 day variations as inferred from 8-year OLR data. *J. Meteor. Soc. Japan,* **64**, 777–786.

Parker, D.E., 1973: Equatorial Kelvin waves at 100 milibars. *Quart. J. Roy. Meteor. Soc.,* **99**, 116–129.

Takahashi, M., 1987: A theory of the slow phase speed of the intraseasonal oscillation using the wave-CISK. *J. Meteor. Soc. Japan,* **65**, 43–49.

Webster, P.J., 1983: Mechanisms of monsoon low-frequency variability: Surface hydrological effects. *J. Atmos. Sci.,* **40**, 2110–2124.

———— and L.C. Chou, 1980: Low frequency transitions of a simple monsoon system. *J. Atmos. Sci.,* **37**, 368–382.

Weickmann, K.M., 1983: Intraseasonal circulation and outgoing longwave radiation modes during northern hemisphere winter. *Mon. Wea. Rev.,* **111**, 1838–1858.

Yamagata, T., 1987: A simple moist model relevant to the origin of intraseasonal disturbances in the tropics. *J. Meteor. Soc. Japan,* **65**, 153–165.

———— and Y. Hayashi, 1984: A simple diagnostic model for the 30–50 day oscillation in the tropics. *J. Meteor. Soc. Japan,* **62**, 709–717.

Yasunari, T., 1980: A quasi-stationary appearance of 30 to 40 day period in the cloudiness fluctuations during the summer monsoon over India. *J. Meteor. Soc. Japan,* **58**, 225–229.

————, 1981: Structure of an Indian summer monsoon system with around 40-day period. *J. Meteor. Soc. Japan,* **59**, 336–354.

熱帯季節内振動の三次元線形レスポンスモデル

林　　良　一

(Geophysical Fluid Dynamics Laboratory／NOAA)

宮　原　三　郎

(九州大学理学部物理教室)

熱帯季節内振動の伝播と構造について三次元線形レスポンスモデルを使って調べ、その結果をFGGE dataの解析結果と比較検討した。

このモデルでは、40日の周期で振動しながら東に進む熱源の存在が仮定されている。仮定された熱源はある一定の経度帯でその振幅が大きく、その他の経度では相対的に小さな振幅しか持たない。しかしながら、zonal windの応答は、かなりの大きさの東進しながら地球を一周する成分を持っている。また、この振幅は大きな加熱経度帯の中に、節を持っている。これらの構造は、FGGE dataの解析の結果と良く一致している。加熱域が完全に、ある経度帯に限られたときには、少なくともこのモデルで使われた熱源分布では、zonal windの振動はそこから東西に向かって伝播する。

大気の応答のなかの東進する波数1成分は、上部対流圏ではKelvin-Rossby modeの結合体の形を取り、下部対流圏ではRossby modeがその主な成分となっている。また、下部対流圏での構造は、境界層内での子午面循環によって変形されたwalker cellの構造をも持っている。これらの構造は、FGGE dataの解析の結果とも良く一致している。下部対流圏におけるRossby modeの卓越は地表面摩擦の影響によるものであることが確かめられた。